An Efficient Analysis of Planar Microwave Circuits Using A DWT-Based HAAR MRTD Scheme

Guillaume Carat, Raphaël Gillard, Jacques Citerne, *Member, IEEE*, and Joe Wiart, *Member, IEEE*

***Abstract*—A new wavelet-based technique to generate multiresolution time-domain schemes is presented in this paper. By using symbolic calculus, a rigorous and general formulation of subgridding at every level of multiresolution is obtained. As it is rigorously equivalent to a finer finite-difference time-domain (FDTD) scheme, it does not require any particular treatments for boundary conditions. This technique has been successfully applied to the study of microstrip structures. The near- and the far-field computation can be both improved in terms of CPU time and memory storage, while maintaining the same accuracy as the classical FDTD computation.**

***Index Terms*—Far-field computation, FDTD methods, Haar transforms, microstrip antennas, microstrip circuits, multiresolution analysis, subgridding, wavelet transforms.**

I. Introduction

THE use of wavelets has already been demonstrated to reduce the computer requirements (CPU time and memory storage) when performing the electromagnetic analysis of large structures [1], [2]. Recently, multiresolution time-domain (MRTD) schemes have been introduced [3], [4] by using the Galerkin's formalism. The main interest of the MRTD scheme is the new repartition of the information held by a field component. The information is now split between an average value (scale component) and details values (wavelets components). The point is now the possibility to neglect wavelet components that naturally leads to a coarser finite-difference time-domain (FDTD) scheme. That thresholding is done at particular locations in the computation volume, which naturally defines a subgridding process. Nevertheless, due to the complexity of its usual formulation (lots of different basis functions), the construction of MRTD schemes cannot be generalized easily at any level of multiresolution. Moreover, as shown in [5] and [6], MRTD boundary conditions usually need particular treatments. This can be related to the fact that the schemes are not equivalent to finer FDTD schemes. As a result, MRTD schemes seem to be difficult to obtain for every level of multiresolution.

In this paper, we propose a new way to derive a MRTD scheme from a classical FDTD scheme by using symbolic calculus with a discrete wavelet transform (DWT) based on the Haar Wavelet [7]. A wavelet transform is directly applied on the FDTD update equations without using the Galerkin's formalism. New MRTD update equations are then obtained for every level of multiresolution. This procedure has the advantage to rely on a very general formulation. It is applicable to any level of multiresolution. It does not require any particular treatment when boundary conditions are involved because the MRTD update equations are automatically constructed from a classical FDTD description of the studied structure at a finer level (in which all boundary conditions are described as usual). As a result, the obtained MRTD scheme is strictly equivalent to that fine FDTD scheme. The subgridding process can also be included in the symbolic calculus phase: practically, the update equations for wavelet components to be neglected can be *a priori* removed from the set of equations generated by symbolic calculus. The whole procedure permits to automatically obtain an MRTD scheme whose update equations are matched to any desired structure with any desired level of multiresolution and any desired subgridding. This technique was first initiated in [8] using a one-dimensional (1-D) multiresolution.

To sum up, we describe a more general formulation that is suitable for both 1-D and two-dimensional (2-D) multiresolution schemes in three-dimensional (3-D) FDTD codes. It could be easily extended to 3-D MRTD schemes if required. We also propose a new way of using wavelets to reduce computer requirements in near- to far-field transformations. Such a compression has already been obtained by using an additional DWT procedure in the classical FDTD method [9]. Nevertheless, the near field calculation could not be improved by this procedure. As a validation, we applied the proposed method to the study of a microstrip filter and to the near- and far-field calculation for a microstrip antenna.

II. Principle of the 1-D MRTD Scheme

A. General Update Equation for the FDTD Field Computation

Here, we introduce a general formulation for the updating of the field components in the classical FDTD scheme. This formulation is shown to be suitable for any point in the computation volume whatever the particular conditions at this point.

As an example, let us consider the proposed update equation for the E_x-field component

$$\begin{aligned} E^{n+1}_{x_{i+(1/2),j,k}} &= \alpha^{E_x}_{i+(1/2),j,k} E^{n}_{x_{i+(1/2),j,k}} \\ &\quad + \beta^{E_x}_{i+(1/2),j,k}\left(H^{n+(1/2)}_{z_{i+(1/2),j+(1/2),k}} - H^{n+(1/2)}_{z_{i+(1/2),j-(1/2),k}}\right) \\ &\quad + \gamma^{E_x}_{i+(1/2),j,k}\left(H^{n+(1/2)}_{y_{i+(1/2),j,k+(1/2)}} - H^{n+(1/2)}_{y_{i+(1/2),j,k-(1/2)}}\right) \\ &\quad + \delta^{E_x}_{i+(1/2),j,k} V^{n+(1/2)}_{s} \end{aligned} \tag{1}$$

Manuscript received March 4, 2000; revised August 21, 2000. This work was supported by France Telecom under Contract 99 1B 113.

G. Carat, R. Gillard, J. Citerne are with the Laboratory for Telecommunication Components and Systems, National Institute of Applied Sciences, 35043 Rennes, France.

J. Wiart is with France Telecom Research and Development, 92794 Issy Les Moulineaux, France.

Publisher Item Identifier S 0018-9480(00)10718-5.

TABLE I
COEFFICIENTS IN THE FDTD SCHEME

Coefficients	$\alpha^{E_x}_{i+\frac{1}{2},j,k}$	$\beta^{E_x}_{i+\frac{1}{2},j,k}$	$\gamma^{E_x}_{i+\frac{1}{2},j,k}$	$\delta^{E_x}_{i+\frac{1}{2},j,k}$
Homogeneous medium (ϵ,μ_0)	1	$\frac{\Delta t}{\epsilon_{i+\frac{1}{2},j,k}\Delta y}$	$-\frac{\Delta t}{\epsilon_{i+\frac{1}{2},j,k}\Delta z}$	0
Lumped resistive voltage generator (R_s,V_s)	$-\frac{1-\frac{\Delta t\Delta x}{2R_s\epsilon_{i+\frac{1}{2},j,k}\Delta z\Delta y}}{1+\frac{\Delta t\Delta x}{2R_s\epsilon_{i+\frac{1}{2},j,k}\Delta z\Delta y}}$	$\frac{\frac{\Delta t}{\epsilon_{i+\frac{1}{2},j,k}\Delta y}}{1+\frac{\Delta t\Delta x}{2R_s\epsilon_{i+\frac{1}{2},j,k}\Delta z\Delta y}}$	$-\frac{\frac{\Delta t}{\epsilon_{i+\frac{1}{2},j,k}\Delta z}}{1+\frac{\Delta t\Delta x}{2R_s\epsilon_{i+\frac{1}{2},j,k}\Delta z\Delta y}}$	$\frac{\frac{\Delta t}{R_s\epsilon_{i+\frac{1}{2},j,k}\Delta z\Delta y}}{1+\frac{\Delta t\Delta x}{2R_s\epsilon_{i+\frac{1}{2},j,k}\Delta z\Delta y}}$
dielectric interface (ϵ^1,μ_0) (ϵ^2,μ_0)	1	$\frac{2\Delta t}{(\epsilon^1_{i+\frac{1}{2},j,k}+\epsilon^2_{i+\frac{1}{2},j,k})\Delta y}$	$-\frac{2\Delta t}{(\epsilon^1_{i+\frac{1}{2},j,k}+\epsilon^2_{i+\frac{1}{2},j,k})\Delta x}$	0

where the coefficients α, β, γ, and δ are structure dependent, and $V_s^{n+(1/2)}$ is representing a possible source term [10].

For a regular point in an homogeneous medium, we assume that

$$\begin{aligned}\alpha_{i+(1/2),j,k} &= 1\\ \beta_{i+(1/2),j,k} &= \frac{\Delta t}{\epsilon_{i+(1/2),j,k}\Delta y}\\ \gamma_{i+(1/2),j,k} &= -\frac{\Delta t}{\epsilon_{i+(1/2),j,k}\Delta z}\\ \delta &= 0\end{aligned}$$

and (1) reduces to the classical FDTD update equation [11].

On the other hand, if we let

$$\alpha_{i+(1/2),j,k} = -\frac{1-\frac{\Delta t\Delta x}{2R_s\epsilon_{i+(1/2),j,k}\Delta z\Delta y}}{1+\frac{\Delta t\Delta x}{2R_s\epsilon_{i+(1/2),j,k}\Delta z\Delta y}}$$

$$\beta_{i+(1/2),j,k} = \frac{\frac{\Delta t}{\epsilon_{i+(1/2),j,k}\Delta y}}{1+\frac{\Delta t\Delta x}{2R_s\epsilon_{i+(1/2),j,k}\Delta z\Delta y}}$$

$$\gamma_{i+(1/2),j,k} = -\frac{\frac{\Delta t}{\epsilon_{i+(1/2),j,k}\Delta z}}{1+\frac{\Delta t\Delta x}{2R_s\epsilon_{i+(1/2),j,k}\Delta z\Delta y}}$$

$$\delta_{i+(1/2),j,k} = \frac{\frac{\Delta t}{R_s\epsilon_{i+(1/2),j,k}\Delta z\Delta y}}{1+\frac{\Delta t\Delta x}{2R_s\epsilon_{i+(1/2),j,k}\Delta z\Delta y}}$$

we have the possibility to account for a lumped source element at that point, as given in [10], [12].

We can also vanish E_x (which is required if the field component is located on a perfect conductor) by choosing

$$\alpha_{i+(1/2),j,k} = \beta_{i+(1/2),j,k} = \gamma_{i+(1/2),j,k} = \delta_{i+(1/2),j,k} = 0.$$

Indeed, we see that any particular treatment can be obtained by a judicious choice of the four coefficient α, β, γ, and δ introduced in (1).

Table I sums up the values of the coefficients for the most usual treatments required in the modeling of planar microwave circuits.

Practically, this general formulation permits to use a single equation for updating all E_x components in the FDTD volume.

By introducing the $\mathbf{H^{n+(1/2)}}$ vector defined by

$$\mathbf{H^{n+(1/2)}} = \begin{pmatrix} H^{n+(1/2)}_{z_{i+(1/2),j-(1/2),k}}\\ H^{n+(1/2)}_{z_{i+(1/2),j+(1/2),k}}\\ H^{n+(1/2)}_{y_{i+(1/2),j,k-(1/2)}}\\ H^{n+(1/2)}_{y_{i+(1/2),j,k+(1/2)}}\end{pmatrix}$$

and the $\mathbf{D}$ vector defined by

$$\mathbf{D} = \begin{pmatrix} -\beta_{i+(1/2),j,k} & \beta_{i+(1/2),j,k} & -\gamma_{i+(1/2),j,k} & \gamma_{i+(1/2),j,k}\end{pmatrix}$$

the update equation (1) can be rewritten as

$$E^{n+1}_{x_{i+(1/2),j,k}} = \alpha^{E_x}_{i+(1/2),j,k}E^{n}_{x_{i+(1/2),j,k}} + \mathbf{D}\mathbf{H^{n+(1/2)}} + \delta^{E_x}_{i+(1/2),j,k}V_s^{n+(1/2)}. \quad (2)$$

Similar equations can be obtained to update the five other fields components.

Only the (α, β, γ, δ) coefficients differ from one cell to the other and from one component to the other.

B. DWT-Based MRTD Formulation

We now propose to use a DWT transform to obtain a new MRTD scheme. We first recall that the classical FDTD scheme can be seen as a decomposition of the fields components using pulse basis functions [3]. From the multiresolution viewpoint, these functions correspond to the scale functions of the Haar basis [7]. As a consequence, a DWT transform can be used to convert those fields components and to obtain a decomposition with both scale and wavelet functions at a coarser level. We propose to apply this DWT transform directly to the classical FDTD update equations (2) and not to numerical computed values. This directly yields to the corresponding MRTD update equations. As will be shown later, the main interest of this new approach is the possibility of taking advantage of symbolic calculus to generate automatically MRTD schemes for complex structures.

For the sake of simplicity, we first restrict the presentation to a 1-D DWT transform. This means that although we use a 3-D FDTD scheme, multiresolution is just applied in one particular

direction (y-direction in the following). Practically, M E_x consecutive fields components in the y-direction are used to define an M component vector (with $M = 2^l$ and l the level of wavelet transform)

$$\mathbf{E}_{\mathbf{x}}^{\mathrm{FDTD}^{\mathbf{n+1}}} = \begin{pmatrix} E^{n+1}_{x_{i+(1/2),j,k}} \\ E^{n+1}_{x_{i+(1/2),j+1,k}} \\ \vdots \\ E^{n+1}_{x_{i+(1/2),j+M-1,k}} \end{pmatrix}. \tag{3}$$

(For simplicity, indexes $(i + 1/2, j, k)$ will not be written in the following explanation if they add no significant information). The Haar DWT can be expressed as a simple matrix product

$$\mathbf{E}_{\mathbf{x}}^{\mathrm{MRTD}^{\mathbf{n}}} = W_E \mathbf{E}_{\mathbf{x}}^{\mathrm{FDTD}^{\mathbf{n}}}. \tag{4}$$

W_E is a square $M \times M$ orthogonal matrix representing the 1-D Haar wavelet transform in one direction and $\mathbf{E}_{\mathbf{x}}^{\mathrm{MRTD}^{\mathbf{n}}}$ is the vector formed by the wavelet components obtained after the DWT, at time n.

Using relation (2), the $\mathbf{E}_{\mathbf{x}}^{\mathrm{FDTD}^{\mathbf{n+1}}}$ can be written in the following way:

$$\mathbf{E}_{\mathbf{x}}^{\mathrm{FDTD}^{\mathbf{n+1}}} = D_1 \mathbf{E}_{\mathbf{x}}^{\mathrm{FDTD}^{\mathbf{n}}} + D_2 \mathbf{H}^{\mathrm{FDTD}^{\mathbf{n+(1/2)}}} + D_3 \mathbf{V}_{\mathbf{s}}^{\mathbf{n+(1/2)}} \tag{5}$$

where D_1 (D_3, respectively) is a diagonal matrix of size $M \times M$ composed by the α (δ coefficients, respectively) given by

$$D_1 = \begin{pmatrix} \alpha_{i+(1/2),j,k} & 0 & \cdots & 0 \\ 0 & \alpha_{i+(1/2),j+1,k} & \ddots & \vdots \\ \vdots & \ddots & \ddots & 0 \\ 0 & \cdots & 0 & \alpha_{i+(1/2),j+M-1,k} \end{pmatrix}$$

and D_2 is a nonsquare $M \times (3M + 1)$ matrix defined by the equation shown at the bottom of this page.

Combining (4) and (5), we obtain

$$\mathbf{E}_{\mathbf{x}}^{\mathrm{MRTD}^{\mathbf{n+1}}} = W_E D_1 \mathbf{E}_{\mathbf{x}}^{\mathrm{FDTD}^{\mathbf{n}}} + W_E D_2 \mathbf{H}^{\mathrm{FDTD}^{\mathbf{n+(1/2)}}} + W_E D_3 \mathbf{V}_{\mathbf{s}}^{\mathrm{FDTD}^{\mathbf{n+(1/2)}}} \tag{6}$$

where

$$\mathbf{E}_{\mathbf{x}}^{\mathrm{MRTD}^{\mathbf{n+1}}} = \begin{pmatrix} E^{\phi^{n+1}_{l,0}}_{x_{i+(1/2),j_W,k}} \\ \cdots\cdots\cdots\cdots \\ E^{\psi^{n+1}_{l,0}}_{x_{i+(1/2),j_W,k}} \\ \cdots\cdots\cdots\cdots \\ E^{\psi^{n+1}_{l-1,0}}_{x_{i+(1/2),j_W,k}} \\ E^{\psi^{n+1}_{l-1,1}}_{x_{i+(1/2),j_W,k}} \\ \cdots\cdots\cdots\cdots \\ \cdots\cdots\cdots\cdots \\ E^{\psi^{n+1}_{l-i,0}}_{x_{i+(1/2),j_W,k}} \\ E^{\psi^{n+1}_{l-i,2^i-1}}_{x_{i+(1/2),j_W,k}} \\ \cdots\cdots\cdots\cdots \\ \cdots\cdots\cdots\cdots \\ E^{\psi^{n+1}_{1,0}}_{x_{i+(1/2),j_W,k}} \\ E^{\psi^{n+1}_{1,2^l-1-1}}_{x_{i+(1/2),j_W,k}} \end{pmatrix} \Bigg\updownarrow M$$

and

$$\mathbf{H}^{\mathrm{FDTD}^{\mathbf{n+(1/2)}}} = \begin{pmatrix} H^{n+(1/2)}_{z_{i+(1/2),j-(1/2),k}} \\ H^{n+(1/2)}_{z_{i+(1/2),j+(1/2),k}} \\ \cdots\cdots\cdots\cdots \\ H^{n+(1/2)}_{z_{i+(1/2),j+(M-1/2),k}} \\ \cdots\cdots\cdots\cdots \\ H^{n+(1/2)}_{y_{i+(1/2),j,k-(1/2)}} \\ \cdots\cdots\cdots\cdots \\ H^{n+(1/2)}_{y_{i+(1/2),j+M-1,k-(1/2)}} \\ \cdots\cdots\cdots\cdots \\ H^{n+(1/2)}_{y_{i+(1/2),j,k+(1/2)}} \\ \cdots\cdots\cdots\cdots \\ H^{n+(1/2)}_{y_{i+(1/2),j+M-1,k+(1/2)}} \end{pmatrix} \Bigg\updownarrow 3M+1 = \begin{matrix} \Big\updownarrow M+1 \\ \Big\updownarrow M \\ \Big\updownarrow M \end{matrix}$$

where we use index notation j_W for numerotation in the MRTD scheme, defined by

$$j_W = E\left(\frac{j+1}{M}\right)$$

with $E(x)$ the integer part of x. $E_x^{\psi_{l',l''}}$ are the wavelets components (l' is the index of dilatation, l'' is the index of translation),

$$D_2 = \begin{pmatrix} -\beta_j & \beta_j & 0 & \cdots & 0 & -\gamma_j & 0 & \cdots & 0 & \gamma_j & 0 & \cdots & 0 \\ 0 & -\beta_{j+1} & \beta_{j+1} & \ddots & \vdots & 0 & -\gamma_{j+1} & 0 & \ddots & 0 & \gamma_{j+1} & \ddots & \vdots \\ \vdots & \ddots & \ddots & \ddots & 0 & \vdots & \ddots & \ddots & \ddots & \ddots & \ddots & \ddots & 0 \\ 0 & \cdots & 0 & -\beta_{j+M-1} & \beta_{j+M-1} & 0 & \cdots & 0 & -\gamma_{j+M-1} & 0 & \cdots & 0 & \gamma_{j+M-1} \end{pmatrix}$$

and $E_x^{\phi_{l,0}}$ is the scale component (functions ψ, ϕ are defined as in [7]).

The vector $\mathbf{V_s^{n+(1/2)}}$ is defined in the same way as the vector $\mathbf{E_x^{FDTD^n}}$.

We also have

$$\mathbf{E_x^{FDTD^n}} = W_E^{-1}\mathbf{E_x^{MRTD^n}} \tag{7}$$

and

$$\mathbf{H^{FDTD^{n+(1/2)}}} = W_H^{-1}\mathbf{H^{MRTD^{n+(1/2)}}} \tag{8}$$

where

$$\mathbf{H^{MRTD^{n+(1/2)}}} = \begin{pmatrix} (\mathbf{H^{MRTD^{n+(1/2)}}_{Z_{i+(1/2),j_W-(1/2),k}}}) \\ (\mathbf{H^{MRTD^{n+(1/2)}}_{Z_{i+(1/2),j_W+(1/2),k}}}) \\ (\mathbf{H^{MRTD^{n+(1/2)}}_{y_{i+(1/2),j_W,k-(1/2)}}}) \\ (\mathbf{H^{MRTD^{n+(1/2)}}_{y_{i+(1/2),j_W,k+(1/2)}}}) \end{pmatrix} \Big\updownarrow 4M$$

and W_H^{-1} is a block $(3M+1)\times(4M)$ matrix defined by

$$W_H^{-1} = \begin{pmatrix} W_E^{\boldsymbol{l}} & 0 & \cdots & 0 \\ 0 & W_E^{-1} & 0 & 0 \\ 0 & 0 & W_E^{-1} & 0 \\ 0 & 0 & 0 & W_E^{-1} \end{pmatrix} \begin{matrix} \updownarrow 1 \\ \\ \\ \updownarrow 3M \end{matrix}$$

where $W_E^{\boldsymbol{l}}$ is the last row of the W_E^{-1} matrix.

This matrix expresses the inverse DWT for the $\mathbf{H^{MRTD^{n+(1/2)}}}$ vector. It is different from W_E^{-1} because the vector dimension and arrangement are not the same. $W_E^{-1} = W_E^t$, thanks to the property of orthogonality of the W_E matrix.

By using relation (7) and (8) in (6), we then obtain the fundamental equation

$$\begin{aligned} \mathbf{E_x^{MRTD^{n+1}}} &= W_E D_1 W_E^{-1}\mathbf{E_x^{MRTD^n}} \\ &\quad + W_E D_2 W_H^{-1}\mathbf{H^{MRTD^{n+(1/2)}}} \\ &\quad + W_E D_3 W_E^{-1}\mathbf{V_S^{MRTD^{n+(1/2)}}}. \end{aligned} \tag{9}$$

This matrix equation provides the update scheme for each MRTD E_x component.

For example, the update equation obtained for the $E_{x_{i+(1/2),j_W,k}}^{\phi_{l,0}^{n+1}}$ component is

$$\begin{aligned} E_{x_{i+(1/2),j_W,k}}^{\phi_{l,0}^{n+1}} &= \sum_{p=0}^{M-1}\left((\mathbf{E_x^{MRTD^n}})_p \sum_{q=0}^{M-1}(h_{p,q}\alpha_{i+(1/2),j+q,k})\right) \\ &\quad + \left((\mathbf{H^{MRTD^{n+(1/2)}}_{Z_{i+(1/2),j_W-(1/2),k}}})_{M-1} \cdot \sum_{q=0}^{M-1}(h_{M-1,q}\beta_{i+(1/2),j+q-M-1,k})\right) \\ &\quad + \sum_{p=0}^{M-1}\left((\mathbf{H^{MRTD^{n+(1/2)}}_{Z_{i+(1/2),j_W+(1/2),k}}})_p \cdot \sum_{q=0}^{M-1}(h_{p,q}\beta_{i+(1/2),j+q,k})\right) \\ &\quad + \sum_{p=0}^{M-1}\left((\mathbf{H^{MRTD^{n+(1/2)}}_{y_{i+(1/2),j_W,k-(1/2)}}})_p \cdot \sum_{q=0}^{M-1}(h_{p,q}\gamma_{i+(1/2),j+q,k-1})\right) \\ &\quad + \sum_{p=0}^{M-1}\left((\mathbf{H^{MRTD^{n+(1/2)}}_{y_{i+(1/2),j_W,k+(1/2)}}})_p \cdot \sum_{q=0}^{M-1}(h_{p,q}\gamma_{i+(1/2),j+q,k})\right) \end{aligned} \tag{10}$$

where $(h_{p,q})_{p,q=0,\ldots,M-1}$ is the general term of the Haar matrix W_E, and $(A)_p$ is the p component from the A vector (with A equals to $\mathbf{E}$ or $\mathbf{H}$). It should be noticed that the generated scheme is a coupled scheme between ψ and ϕ components of electromagnetic fields.

The second term of this expression

$$\left[(\mathbf{H^{MRTD^{n+(1/2)}}_{Z_{i+(1/2),\,j_W-(1/2),\,k}}})_{M-1} \sum_{q=0}^{M-1}(h_{M-1,q}\beta_{i+(1/2),j+q-M-1,k})\right]$$

comes from the fact that the $H_{z_{i+(1/2),j-(1/2),k}}^{n+(1/2)}$ FDTD component is inside the (i, j_W-1, k) MRTD cell, and not inside the (i, j_W, k) MRTD cell like other $H_{z_{i+(1/2),j'+(1/2),k}}^{n+(1/2)}$ components (see Fig. 1). As shown above, (9) provides a compact form for the whole MRTD scheme.

It can be seen that these update equations are general and that the particular physical conditions associated with a given point (dielectric interface, ...) are included in the D_i matrix thanks to (4).

As a consequence, no particular treatments have to be added to account for specific boundary conditions. Perfectly matched layer (PML) conditions can be obtained directly by this technique. Nevertheless, as Mur first-order absorbing boundary conditions (ABCs) were directly available in our FDTD code, corresponding MRTD conditions were derived, by solving a linear system of order M (that system comes from the semiimplicit formulation of those conditions).

One must also keep in mind that, by construction, such an MRTD scheme is completely equivalent to a classical FDTD scheme at a finer level. This property was not verified in previously published MRTD schemes [3], [4].

This equivalence can be released when wavelet components are neglected in the MRTD scheme. This usually permits to reduce the computer requirements without sacrificing the accuracy. Indeed, although this scheme seems to be more complicated than the FDTD one ($6M$ different update equations against six update equations), it has the great property to concentrate most of information on the scale component (indexed by $\phi_{\boldsymbol{l},0}$). It subsequently gives a rigorous formulation of subgridding.

To illustrate, we consider the example with a level $l = 2$ of multiresolution ($M = 4$).

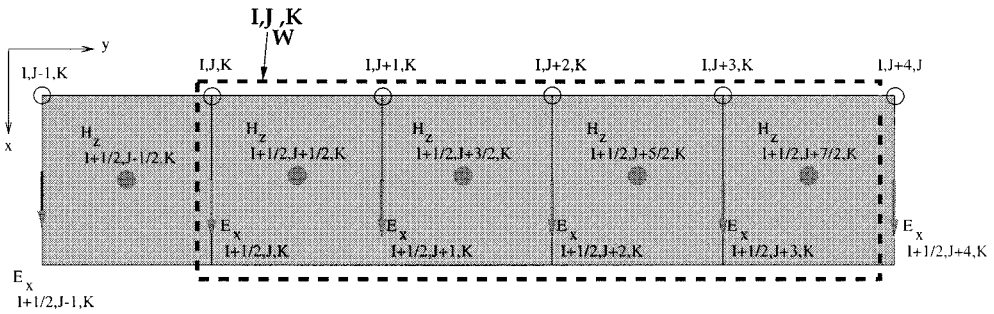

Fig. 1. Example of 1-D y-coarse grid supported by the fine grid.

In this case, the Haar matrix W_E is given by

$$W_E = \begin{pmatrix} (1/2) & (1/2) & (1/2) & (1/2) \\ (1/2) & (1/2) & -(1/2) & -(1/2) \\ \frac{1}{\sqrt{2}} & -\frac{1}{\sqrt{2}} & 0 & 0 \\ 0 & 0 & \frac{1}{\sqrt{2}} & -\frac{1}{\sqrt{2}} \end{pmatrix} \tag{11}$$

and the update equation (10), in an homogeneous case, reduces to

$$\begin{aligned} E^{\phi_{2,0}^{n+1}}_{x_{i+(1/2),j_W,k}} &= E^{\phi_{2,0}^{n}}_{x_{i+(1/2),j_W,k}} + \frac{\Delta t}{\epsilon} \\ &\cdot \left(\frac{H^{\phi_{2,0}^{n+(1/2)}}_{z_{i+(1/2),j_W+(1/2),k}} - H^{\phi_{2,0}^{n+(1/2)}}_{z_{i+(1/2),j_W-(1/2),k}}}{4\Delta y} \right. \\ &- \frac{H^{\psi_{2,0}^{n+(1/2)}}_{z_{i+(1/2),j_W+(1/2),k}} - H^{\psi_{2,0}^{n+(1/2)}}_{z_{i+(1/2),j_W-(1/2),k}}}{4\Delta y} \\ &- \frac{H^{\psi_{1,1}^{n+(1/2)}}_{z_{i+(1/2),j_W+(1/2),k}} - H^{\psi_{1,1}^{n+(1/2)}}_{z_{i+(1/2),j_W-(1/2),k}}}{2\sqrt{2}\Delta y} \\ &- \left. \frac{H^{\phi_{2,0}^{n+(1/2)}}_{y_{i+(1/2),j_W,k+(1/2)}} - H^{\phi_{2,0}^{n+(1/2)}}_{y_{i+(1/2),j_W,k-(1/2)}}}{\Delta z} \right). \end{aligned} \tag{12}$$

By neglecting all wavelet functions in this update equation ($\psi_{2,0}$, $\psi_{1,1}$), a four times coarser FDTD scheme in the y-direction is obtained as follows:

$$\begin{aligned} E^{\phi_{2,0}^{n+1}}_{x_{i+(1/2),j_W,k}} &= E^{\phi_{2,0}^{n}}_{x_{i+(1/2),j_W,k}} + \frac{\Delta t}{\epsilon} \\ &\cdot \left(\frac{H^{\phi_{2,0}^{n+(1/2)}}_{z_{i+(1/2),j_W+(1/2),k}} - H^{\phi_{2,0}^{n+(1/2)}}_{z_{i+(1/2),j_W-(1/2),k}}}{4\Delta y} \right. \\ &- \left. \frac{H^{\phi_{2,0}^{n+(1/2)}}_{y_{i+(1/2),j_W,k+(1/2)}} - H^{\phi_{2,0}^{n+(1/2)}}_{y_{i+(1/2),j_W,k-(1/2)}}}{\Delta z} \right). \end{aligned}$$

This scheme reduces to a classical FDTD scheme with a space step in the y-direction equal to $4\Delta y$. Such an approximation can be used to define a local coarse FDTD grid in the y-direction.

C. Numerical Implementation

A last remark concerns the practical implementation of this new MRTD scheme. Although general, (10) would be very time and memory consuming if programmed directly (a lot of matrix coefficients would be required at each time step and at each field component). In practice, it is much more efficient to replace this formal coefficients by their numerical values (this drastically simplifies the equations as many zero coefficients are usually involved). To do so, symbolic calculus is used to automatically construct a specific implementation for each new structure. This preprocessing step is very rapid and permits to largely improve the simulation process. Practically, we first use a classical FDTD interface to describe the studied structure. This permits to obtain all the α, β, δ, and γ coefficients that are required in the D_i matrices. We then construct the update equations for each field components in the FDTD volume using (10). Indeed, sets of fields components with similar update equations are used to reduce the total amount of update equations. (For example, all the E_x components in an homogeneous medium will have the same update equations and will be grouped in the same set). This construction of the MRTD scheme is done using symbolic calculus. When subgridding is involved, it must be directly dealt with during this process. The obtained source code is then compiled, linked, and executed.

III. Principle of a 2-D MRTD Scheme

The 2-D MRTD scheme is derived like the 1-D MRTD scheme.

The first step of the derivation is the same as explained before, with the use of structure-dependent coefficients α, β, γ, and δ.

The second step now implies a 2-D DWT on the classical FDTD update equation. l_x (l_y, respectively) is the level of multiresolution in the x(y-direction, respectively).

A matrix $E_x^{FDTD^{n+1}}$ of size $M_x \times M_x M_y$ is defined by taking E_x consecutive fields component in the x- and y-directions (with $M_x = 2^{l_x}$ and $M_y = 2^{l_y}$).

By noting

$$V_{i,k}^{n+1} = \begin{pmatrix} E^{n+1}_{x_{i+(1/2),j,k}} \\ E^{n+1}_{x_{i+(1/2),j+1,k}} \\ \vdots \\ E^{n+1}_{x_{i+(1/2),j+M_y-1,k}} \end{pmatrix}$$

we define

$$\mathbf{E}_{\mathbf{x}}^{\mathrm{FDTD}^{\mathbf{n+1}}} = \begin{pmatrix} V_{i,k} & 0 & \cdots & 0 \\ 0 & V_{i+1,k} & 0 & \vdots \\ \vdots & 0 & \ddots & 0 \\ 0 & \cdots & 0 & V_{i+M_x-1,k} \end{pmatrix}. \quad (13)$$

The Haar 2-D DWT can now be expressed by

$$\mathbf{E}_{\mathbf{x}}^{\mathrm{MRTD}^{\mathbf{n}}} = W_{E_{(j)}}^{2D}\, \mathbf{E}_{\mathbf{x}}^{\mathrm{FDTD}^{\mathbf{n}}} W_{E_{(i)}}^{2D^{-1}} \quad (14)$$

where $\mathbf{E}_{\mathbf{x}}^{\mathrm{MRTD}^{\mathbf{n}}}$ is a matrix of size $M_x \times M_x M_y$, $W_{E_{(j)}}^{2D}$ ($W_{E_{(i)}}^{2D^{-1}}$, respectively) expresses the DWT in the y-direction (x-direction, respectively). Matrices $W_{E_{(i)}}^{2D}$ and $W_{E_{(j)}}^{2D}$ are block matrices built from the W_E Haar matrix. We take here $W_{E_{(i)}}^{2D} = W_E$ (size $M_x \times M_x$) and $W_{E_{(j)}}^{2D} = (W_E \;\; W_E, \ldots, W_E)$ (matrix of size $M_y^2 \times M_y$). We also have

$$\mathbf{H}^{\mathrm{FDTD}^{\mathbf{n+(1/2)}}} = W_{H_{(j)}}^{2D^{-1}} \mathbf{H}^{\mathrm{MRTD}^{\mathbf{n+(1/2)}}} W_{E_{(i)}}^{2D}. \quad (15)$$

This last relation implies W_E^{2D} and W_H^{2D} because of the particular form of the $\mathbf{H}^{\mathrm{FDTD}^{\mathbf{n+(1/2)}}}$ matrix. The relation (5) is now

$$\mathbf{E}_{\mathbf{x}}^{\mathrm{FDTD}^{\mathbf{n+1}}} = D_1 \mathbf{E}_{\mathbf{x}}^{\mathrm{FDTD}^{\mathbf{n}}} + D_2 \mathbf{H}^{\mathrm{FDTD}^{\mathbf{n+(1/2)}}} + D_3 \mathbf{V}_{\mathbf{S}^{\mathbf{n+(1/2)}}} \quad (16)$$

where $\mathbf{H}^{\mathrm{FDTD}^{\mathbf{n+(1/2)}}}$ is a matrix of size $M_x \times M_x(3M_y+1)$ obtained by the same way as the $\mathbf{E}_{\mathbf{x}}^{\mathrm{FDTD}^{\mathbf{n}}}$ matrix and $\mathbf{V}_{\mathbf{s}}^{\mathbf{n+(1/2)}}$ is a $M_x \times M_x M_y$ matrix.

Matrices D_1, D_2, and D_3 are block diagonal matrices built from the $D1$, $D2$, and $D3$ matrices used in the 1-D MRTD scheme.

The dimension of $\mathbf{H}^{\mathrm{FDTD}^{\mathbf{n+(1/2)}}}$ is $M_x \times M_x(3M_y+1)$ because the update equation for the E_x component involves the y- and z-components of H. [The $\mathbf{H}^{\mathrm{FDTD}^{\mathbf{n+(1/2)}}}$ matrix for the E_z update equation has the size $(3M_x+1)\times(3M_x+1)\,(3M_y+1)$].

By applying a $2D$ wavelet transform to relation (16), we then obtain

$$\begin{aligned}\mathbf{E}_{\mathbf{x}}^{\mathrm{MRTD}^{\mathbf{n+1}}} &= W_E^{2D} D_1 W_E^{2D^{-1}} \mathbf{E}_{\mathbf{x}}^{\mathrm{MRTD}^{\mathbf{n}}} \\ &\quad + W_E^{2D} D_2 W_H^{2D^{-1}} \mathbf{H}^{\mathrm{MRTD}^{\mathbf{n+(1/2)}}} \\ &\quad + W_E^{2D} D_3 W_E^{2D^{-1}} \mathbf{V}_{\mathbf{s}}^{\mathrm{MRTD}^{\mathbf{n+(1/2)}}} \end{aligned} \quad (17)$$

that is exactly the same equation as (9), but with matrices and not only vectors.

Similar matricial equations are obtained for the other electromagnetic components. The new 2-D MRTD scheme obtained is more complicated than the 1-D MRTD one ($6M_xM_y$ equations against $6M_y$). Nevertheless, it leads to a 2-D subgridding.

As an example, for $l = l_x = l_y = 1$, the W_E matrix is given by

$$W_E = \begin{pmatrix} \frac{1}{\sqrt{2}} & \frac{1}{\sqrt{2}} \\ \frac{1}{\sqrt{2}} & -\frac{1}{\sqrt{2}} \end{pmatrix} \quad (18)$$

and M_xM_y update equations obtained for the E_x component are

$$\begin{aligned} E_{x_{i_W+(1/2),j_W,k}}^{\phi^x \phi^{y^{n+1}}} &= E_{x_{i_W+(1/2),j_W,k}}^{\phi^x \phi^{y^n}} + \frac{\Delta t}{\epsilon} \cdot \left(\frac{H_{z_{i_W+(1/2),j_W+(1/2),k}}^{\phi^x \phi^{y^{n+(1/2)}}} - H_{z_{i_W+(1/2),j_W-(1/2),k}}^{\phi^x \phi^{y^{n+(1/2)}}}}{2\Delta y} \right. \\ &\quad - \frac{H_{z_{i_W+(1/2),j_W+(1/2),k}}^{\phi^x \psi^{y^{n+(1/2)}}} - H_{z_{i_W+(1/2),j_W-(1/2),k}}^{\phi^x \psi^{y^{n+(1/2)}}}}{2\Delta y} \\ &\quad \left. + \frac{H_{y_{i_W+(1/2),j_W,k+(1/2)}}^{\phi^x \phi^{y^{n+(1/2)}}} - H_{y_{i_W+(1/2),j_W,k-(1/2)}}^{\phi^x \phi^{y^{n+(1/2)}}}}{\Delta z} \right) \end{aligned} \quad (19)$$

$$\begin{aligned} E_{x_{i_W+(1/2),j_W,k}}^{\phi^x \psi^{y^{n+1}}} &= E_{x_{i_W+(1/2),j_W,k}}^{\phi^x \psi^{y^n}} + \frac{\Delta t}{\epsilon} \cdot \left(\frac{H_{z_{i_W+(1/2),j_W+(1/2),k}}^{\phi^x \phi^{y^{n+(1/2)}}} - H_{z_{i_W+(1/2),j_W-(1/2),k}}^{\phi^x \phi^{y^{n+(1/2)}}}}{2\Delta y} \right. \\ &\quad + \frac{3H_{z_{i_W+(1/2),j_W+(1/2),k}}^{\phi^x \psi^{y^{n+(1/2)}}} + H_{z_{i_W+(1/2),j_W-(1/2),k}}^{\phi^x \psi^{y^{n+(1/2)}}}}{2\Delta y} \\ &\quad \left. + \frac{H_{y_{i_W+(1/2),j_W,k+(1/2)}}^{\phi^x \psi^{y^{n+(1/2)}}} - H_{y_{i_W+(1/2),j_W,k-(1/2)}}^{\phi^x \psi^{y^{n+(1/2)}}}}{\Delta z} \right) \end{aligned} \quad (20)$$

$$\begin{aligned} E_{x_{i_W+(1/2),j_W,k}}^{\psi^x \phi^{y^{n+1}}} &= E_{x_{i_W+(1/2),j_W,k}}^{\psi^x \phi^{y^n}} + \frac{\Delta t}{\epsilon} \cdot \left(\frac{H_{z_{i_W+(1/2),j_W+(1/2),k}}^{\psi^x \phi^{y^{n+(1/2)}}} - H_{z_{i_W+(1/2),j_W-(1/2),k}}^{\psi^x \phi^{y^{n+(1/2)}}}}{2\Delta y} \right. \\ &\quad - \frac{H_{z_{i_W+(1/2),j_W+(1/2),k}}^{\psi^x \psi^{y^{n+(1/2)}}} - H_{z_{i_W+(1/2),j_W-(1/2),k}}^{\psi^x \psi^{y^{n+(1/2)}}}}{2\Delta y} \\ &\quad \left. + \frac{H_{y_{i_W+(1/2),j_W,k+(1/2)}}^{\psi^x \phi^{y^{n+(1/2)}}} - H_{y_{i_W+(1/2),j_W,k-(1/2)}}^{\psi^x \phi^{y^{n+(1/2)}}}}{\Delta z} \right) \end{aligned} \quad (21)$$

$$\begin{aligned} E_{x_{i_W+(1/2),j_W,k}}^{\psi^x \psi^{y^{n+1}}} &= E_{x_{i_W+(1/2),j_W,k}}^{\psi^x \psi^{y^n}} + \frac{\Delta t}{\epsilon} \cdot \left(\frac{3H_{z_{i_W+(1/2),j_W+(1/2),k}}^{\psi^x \psi^{y^{n+(1/2)}}} + H_{z_{i_W+(1/2),j_W-(1/2),k}}^{\psi^x \psi^{y^{n+(1/2)}}}}{2\Delta y} \right. \\ &\quad + \frac{H_{z_{i_W+(1/2),j_W+(1/2),k}}^{\psi^x \phi^{y^{n+(1/2)}}} - H_{z_{i_W+(1/2),j_W-(1/2),k}}^{\psi^x \phi^{y^{n+(1/2)}}}}{2\Delta y} \\ &\quad \left. + \frac{H_{y_{i_W+(1/2),j_W,k+(1/2)}}^{\psi^x \psi^{y^{n+(1/2)}}} - H_{y_{i_W+(1/2),j_W,k-(1/2)}}^{\psi^x \psi^{y^{n+(1/2)}}}}{\Delta z} \right) \end{aligned} \quad (22)$$

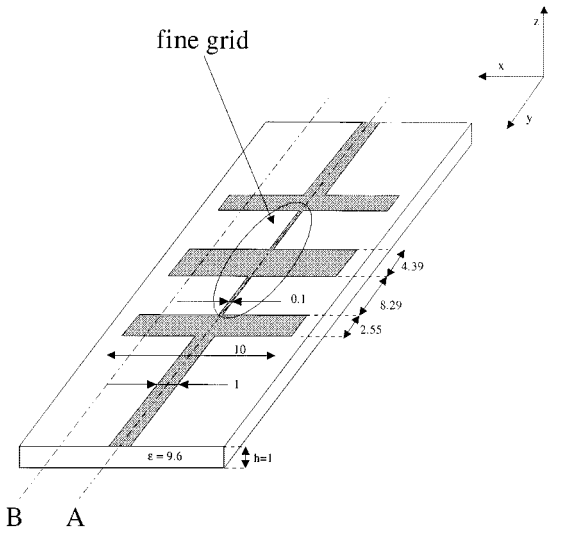

Fig. 2. Low-pass filter (all lengths in millimeters).

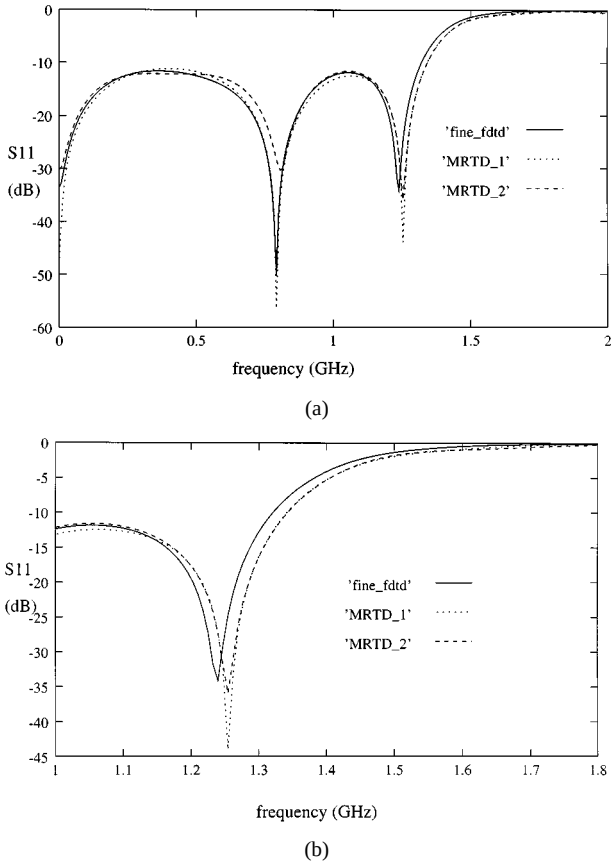

Fig. 3. (a)–(b) Simulations details in the area of the cut off frequency.

(where $\psi = \psi_{1,0}$ and $\phi = \phi_{1,0}$, and for simplicity, indexes were omitted)

A. Numerical Results

To validate the new MRTD scheme, two different structures have been tested: a low-pass filter and a patch antenna with notches.

1) First Validation: Low-Pass Filter: The first studied structure is a microstrip stepped impedance low-pass filter (Fig. 2).

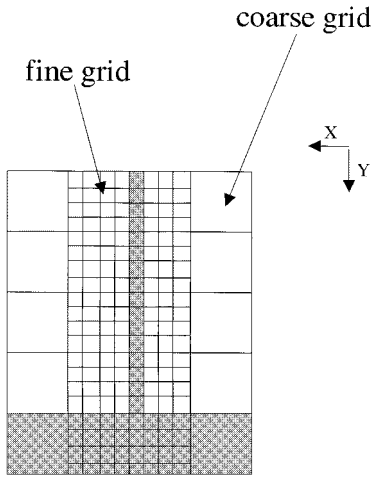

Fig. 4. Fine and coarse grids around the thin line.

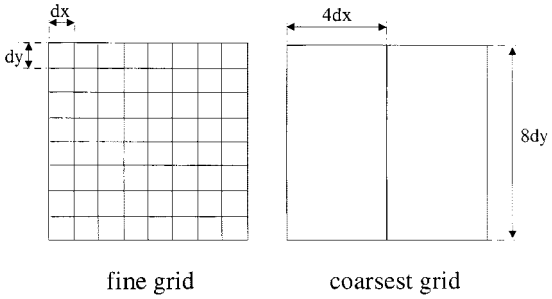

Fig. 5. Difference between fine and coarsest grids in the air.

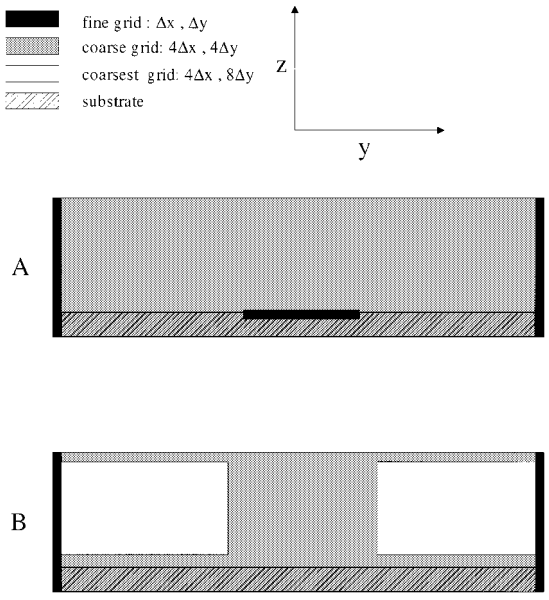

Fig. 6. A and B slices from the low-pass filter (see Fig. 2).

TABLE II
CALCULATION TIME FOR SEVERAL SUBGRIDDINGS

Simulation	Calculation time
fine_fdtd	13h
MRTD_1	1h15
MRTD_2	57min

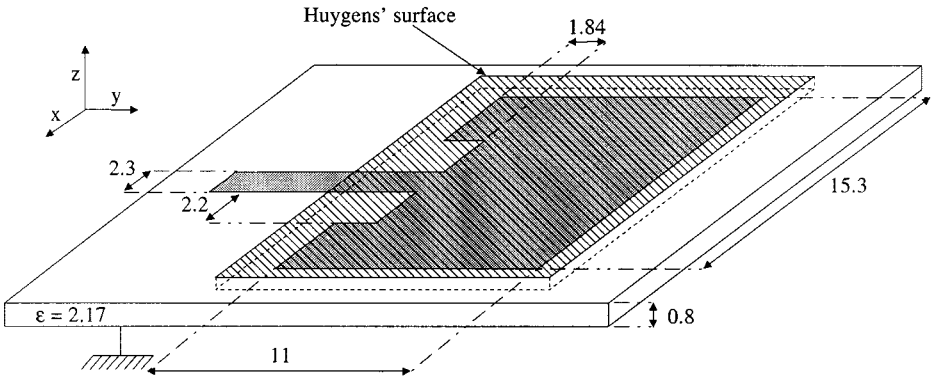

Fig. 7. Tested microstrip antenna.

Simulated results are given in Fig. 3 for the S_{11}-parameter. The analysis of such a structure using a uniform FDTD is highly consuming both in memory storage and in simulation time because the cell size is imposed by the smallest dimension, which is the width of the narrow inductive lines. The resulting mesh size in the x dimension is $d_x = 0.1$ mm ($\lambda_0/750$ at the cutoff frequency $f_c = 1.5$ GHz).

The 2-D MRTD scheme permits to restrict this fine discretization in the vicinity of the inductive lines, as shown in Fig. 2. In the remaining computation volume, a coarser mesh is obtained by neglecting the wavelets components. The reference fine mesh uses $180 \times 600 \times 12$ cells. For the MRTD_1 simulation, the coarse grid is $45 \times 150 \times 12$ (as shown in Fig. 4), with $d_x \simeq \lambda_0/175$, $d_y \simeq \lambda_0/75$. For the MRTD_2 simulation, the precedent coarse grid is also used and a coarsest grid ($45 \times 75 \times 12$) is used (as shown in Figs. 5 and 6), with $d_y \simeq \lambda_0/37$. Results show a great decrease in calculation time for a good accuracy (Fig. 3). They are presented in Table II.

2) Second Validation: Patch Antenna with Notches: This second example shows how the coarse MRTD grid defined above can be used both in near- and far-field computations. Moreover, the far-field computation is drastically reduced by the use of subgridding.

Classically, for the FDTD scheme, a Huygens' surface is defined in the FDTD volume on which equivalent electric and magnetic currents are calculated [13]. Thus, the tangential components of the electric and magnetic fields first have to be stored for each FDTD cell on the Huygens' surface and at any time step (or at a multiple of time step thanks to Shannon's theorem).

A fast Fourier transform is then required to convert each of these field components in the frequency domain. Finally, a near- to far-field computation is performed in the frequency domain, which involves a numerical integration on the Huygens' surface.

It is obvious that the whole post treatment is both memory and time consuming. This is due to the large number of cells on the Huygens' surface that leads to a large number of field components to take into account. However, such a fine grid is not required for the far-field computation. As a consequence, the coarse grid can be used to reduce the cost of this post treatment, which explains the improvement of memory storage and CPU time. This is equivalent to only account for the scale components of the equivalent radiating electric and magnetic currents on the Huygens' surface.

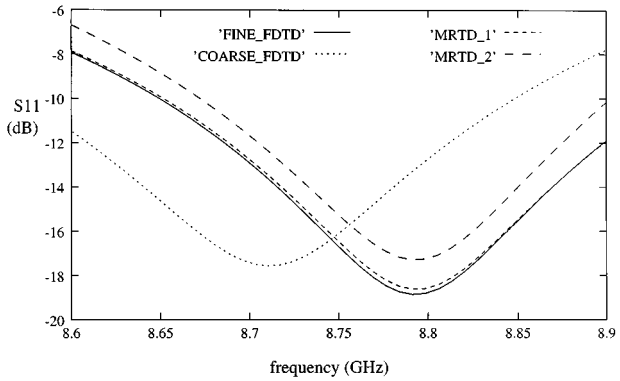

Fig. 8. Examples of several subgridding.

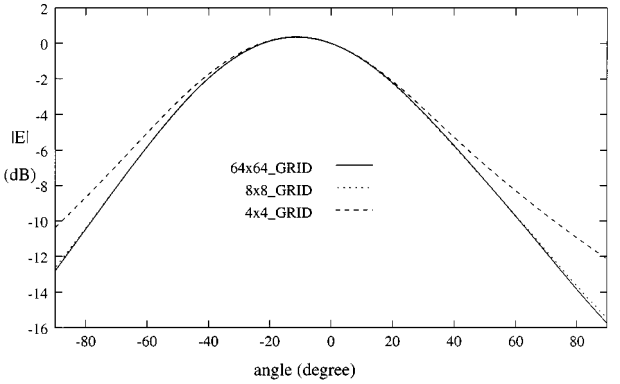

Fig. 9. E-plane copolar.

3) Numerical Results: Simulations are performed for the microstrip structure described in Fig. 7; it is fed with a Gaussian pulse, the fine grid is $70 \times 100 \times 15$ cells, and the cell size is about $\lambda_0/65$ (fine grid) at the resonant frequency (9 GHz). Results for the input return loss are presented in Fig. 8.

For the MRTD_1 simulation, the vicinity of the metallizations is meshed with the fine grid, and the rest of the volume with the coarse grid. The point here is the possibility to get a correct determination of the resonant frequency even with a partial coarse grid. Results show a good agreement between the coarse computation and the fine reference one.

In the MRTD_2 simulation, almost all the volume of calculus is coarse, except the vicinity of the radiating edges of the patch.

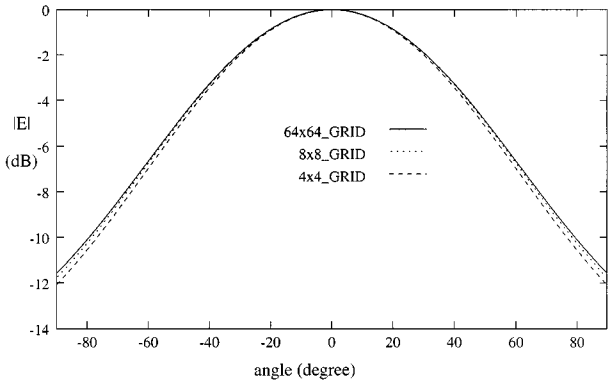

Fig. 10. H-plane copolar.

Results for a coarse FDTD simulation are also given ($70 \times 50 \times 15$ grid).

The resonant frequency is well determined for all MRTD simulations.

MRTD_2 is not so good, which means subgridding must be used carefully. Nevertheless, all MRTD results are much better than the coarse FDTD ones. For the structure, the CPU time for MRTD_2 is divided by two in comparison with the fine FDTD simulation.

In addition to the near-field computation, it is possible to take more advantage of that coarse grid to compute the far fields. The Huygens surface chosen on the fine grid is a 64×64 FDTD cells grid. Then coarse grid induced by the MRTD scheme is used to calculate the far fields.

Results are compared with the one using the whole 64×64 fine grid (the Huygens surface). Figs. 9 and 10 show the corresponding radiating patterns for the E- and H-plane. It should be noticed that no major difference is observed, except for the 4×4 grid. (The 32×32 and 16×16 grids are not presented for clarity, as they give exactly the same results as the 64×64 one). The 4×4 grid exhibits a larger discrepancy that results from an unacceptable level of subgridding. As a consequence, a better compromise is obtained for the 8×8 grid, which corresponds to a reduction factor of 64 in both memory storage and CPU time. Memory storage has decreased from 94 to 1.5 Mb, and the execution time from 8 min to 8 s.

The equivalent grid size is about $\lambda_0/8$, which would not be acceptable in the FDTD volume to compute the near field (it would particularly not be enough to describe the structure and its notches).

IV. Conclusion

A general formulation to obtain MRTD schemes using the DWT has been presented in this paper. Its association with symbolic calculus permits to automatically construct update equations and subgriddings for the study of planar structures. No specific treatments are needed to account for particular boundary conditions and the equivalence with a finer FDTD scheme is rigorous.

This new method has been successfully applied to study microstrip circuits and antennas. Its numerical efficiency is obvious for structures in which geometrical details require a local fine mesh.

The method has also been extended in order to benefit from multiresolution in far-field computations. This largely reduces the computation of radiation patterns in antenna simulation.

References

[1] B. Z. Steinberg and Y. Leviatan, "On the use of wavelet expansions in the method of moments," *IEEE Trans. Antennas Propagat.*, vol. 41, pp. 610–619, Feb. 1993.

[2] R. Loison, R. Gillard, J. Citerne, G. Piton, and H. Legay, "A multi-resolution MoM analysis of multiport structures using matched terminations," *IEEE Trans. Microwave Theory Tech.*, vol. 49, Jan. 2000, to be published.

[3] M. Krumpholz and L. P. B. Katehi, "MRTD: New time-domain schemes based on multiresolution analysis," *IEEE Trans. Microwave Theory Tech.*, vol. 44, pp. 555–571, Apr. 1996.

[4] M. Fujii and W. J. R. Hoefer, "A 3-D Haar-wavelet-based multiresolution analysis similar to the FDTD method—Derivation and application," *IEEE Trans. Microwave Theory Tech.*, vol. 46, pp. 2463–2475, Dec. 1998.

[5] E. M. Tentzeris, R. L. Robertson, J. F. Harvey, and L. P. B. Katehi, "PML absorbing boundary conditions for the characterization of open microwave circuit components using multiresolution time-domain techniques (MRTD)," *IEEE Trans. Antennas Propagat.*, vol. 47, pp. 1709–1715, Nov. 1999.

[6] M. Fujii and W. J. R. Hoefer, "Field singularity correction in 2-D time domain Haar wavelet modeling of waveguide components," in *IEEE MTT-S Int. Microwave Symp. Dig.*, 1999, pp. 1467–1470.

[7] I. Daubechies, *Ten Lectures on Wavelets*. Philadelphia, PA: Soc. Indus. Appl. Math., 1992.

[8] G. Carat, R. Gillard, J. Citerne, and J. Wiart, "A DWT based MRTD scheme using Haar wavelets," in *Millennium Antennas Propagat. Conf.*, Apr. 2000.

[9] G. Carat, R. Gillard, J. Citerne, and J. Wiart, "A discrete wavelet transform (DWT)-based far-field computation using the FDTD method," *Microwave Opt. Technol. Lett.*, vol. 25, no. 4, pp. 241–243, May 2000.

[10] M. J. Picket-May, A. Taflove, and J. Baron, "FDTD modeling of digital signal propagation in 3-D circuits with passive and active loads," *IEEE Trans. Microwave Theory Tech.*, vol. 42, pp. 1514–1523, Aug. 1994.

[11] K. S. Yee, "Numerical solution of initial boundary value problems involving Maxwell's equations in isotropic media," *IEEE Trans. Antennas Propagat.*, vol. AP-14, pp. 302–307, Mar. 1966.

[12] A. Taflove, *Computational Electrodynamics: The Finite-Difference Time-Domain Method*. Norwood, MA: Artech House, 1995.

[13] C. A. Balanis, *Advanced Engineering Electromagnetics*. New York: Wiley, 1989.

Guillaume Carat was born in France, on May 31, 1973. He received the Masters degree in applied mathematics and computer science from the University of Rennes, Rennes, France, in 1998, and is currently working toward the Ph.D. degree in electronics in the Laboratory for Telecommunication Components and Systems (LCST), National Insitute of Applied Sciences (INSA), Rennes, France.

Raphaël Gillard was born June 11, 1966, in France. He received the Diplôme d'Ingénieur and Ph.D. degrees in electronics from the National Insitute of Applied Sciences (INSA), Rennes, France, in 1989 and 1992, respectively.

From August 1992 to September 1993, he was an Engineer in the Ipsis Society, where he was involved with the numerical modeling of millimeter-wave circuits. In October 1993, he joined the Microwave Group of the INSA, where he is currently an Associate Professor. His current research interest concerns numerical methods applied to the computer-aided design (CAD) of microwave circuits and active antennas.

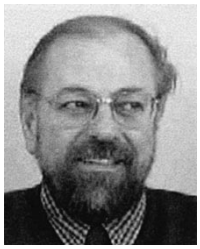

Jacques Citerne (M'98) was born in France, on October 5, 1945. He received the Doctorate degree in physics from the Technical University of Lille, Lille, France, in 1978.

Until 1981, he was the Head of the Circuits and Propagation Group at the Microwave and Semiconductor Center, Technical University of Lille. Since 1981, he has been a Professor of electrical engineering at the National Insitute of Applied Sciences (INSA), Rennes, France, where he has been responsible for the Laboratory for Telecommunication Components and Systems (LCST), which is supported by the French National Center of Scientific Research (CNRS) since 1984. The activities of LCST concern microwave and millimeter-wave circuits and antennas, indoor communications, spread systems, radar, and diffraction.

Joe Wiart (M'96) received the Engineer degree from the Ecole Nationale Supérieure des Télécommunications (ENST), Paris, France, in 1992, and the Ph.D. degree in physics from the ENST and Pierre and Marie Curie University, Paris, France, in 1995.

In 1992, he joined the CNET, the research center of France Telecom, where he spent three years involved with propagation in a microcellular environment. Since 1994, he has been involved with the interaction of radio waves with the human body and on medical electronic devices. He is currently the Head of a group dealing with these questions in the research center of France Telecom. His research interests include electromagnetic compatibility (EMC), bioelectromagnetics, antenna measurements, computational electromagnetics, and signal processing.

Dr. Wiart is Senior member of the Socéité des Electriciens et Electroniciens (SEE). He is vice chairman of the COST 244 bis and chairman of the Federal Office for Scientific, Technical and Cultural Affairs (CENELEC) Working Group in charge of mobile and base-station standards.